# The evolution of the magnetic structures in electron phase-space holes: Two-dimensional particle-in-cell simulations

Mingyu Wu,[1,2] Quanming Lu,[1] Aimin Du,[3] Jinlin Xie,[4] and Shui Wang[1]

Received 20 January 2011; revised 7 July 2011; accepted 14 July 2011; published 12 October 2011.

[1] Observations have shown that electron phase-space holes (electron holes) possess regular magnetic structures. In this paper, two-dimensional (2D) electromagnetic particle-in-cell (PIC) simulations are performed in the ($x$, $y$) plane to study magnetic structures associated with electron holes under different plasma conditions. In the simulations, the background magnetic field ($\mathbf{B}_0 = B_0\vec{\mathbf{e}}_x$) is along the $x$ direction. The combined actions between the transverse instability and stabilization by the background magnetic field lead to the generation of the electric field $E_y$. Then electrons suffer the electric field drift and produce the current in the $z$ direction, which leads to the fluctuating magnetic field along the $x$ and $y$ directions. Meanwhile, the motion of the electron holes along the $x$ direction and the existence of the electric field $E_y$ generate the fluctuating magnetic field along the $z$ direction. In very weakly magnetized plasma ($\Omega_e \ll \omega_{pe}$, where $\Omega_e$ and $\omega_{pe}$ are the electron gyrofrequency and electron plasma frequency, respectively.), the transverse instability is very strong and the magnetic structures associated with electron holes disappear quickly. When $\Omega_e$ is comparable to $\omega_{pe}$, the parallel cut of the fluctuating magnetic field $\delta B_x$ and $\delta B_z$ has unipolar structures in the electron holes, while the parallel cut of fluctuating magnetic field $\delta B_y$ has bipolar structures. In strongly magnetized plasma ($\Omega_e > \omega_{pe}$), electrostatic whistler waves with streaked structures of $E_y$ are excited. The fluctuating magnetic field $\delta B_x$ and $\delta B_z$ also have streaked structures. The relevance between our simulation results and the magnetic structures associated with electron holes observed in the plasma sheet is also discussed.

**Citation:** Wu, M., Q. Lu, A. Du, J. Xie, and S. Wang (2011), The evolution of the magnetic structures in electron phase-space holes: Two-dimensional particle-in-cell simulations, *J. Geophys. Res.*, *116*, A10208, doi:10.1029/2011JA016486.

## 1. Introduction

[2] Electron phase-space holes (electron holes) are often observed in many space environments, such as in the plasma sheet [*Matsumoto et al.*, 1994], auroral zone [*Ergun et al.*, 1998a, 1998b; *Franz et al.*, 1998], magnetosheath [*Pickett et al.*, 2004], magnetopause [*Cattell et al.*, 2002], the transition region of the bow shock [*Bale et al.*, 1998], and solar wind [*Mangeney et al.*, 1999]. In these space-based measurements, they are positive potential pulses, and detected as bipolar electric field signals parallel to the background magnetic field. Electron holes have also been observed in laboratory plasmas, for example, in a magnetized plasma surrounded by a waveguide [*Saeki et al.*, 1979], an unmagnetized laser-generated plasma [*Sarri et al.*, 2010] and during the magnetic reconnection experiments in laboratory [*Fox et al.*, 2008]. Electron holes play an important role in a number of plasma processes, like double layers [*Newman et al.*, 2001] and magnetic reconnection [*Drake et al.*, 2003].

[3] Electron holes are considered to be the stationary BGK solution of Vlasov and Poisson equations [*Bernstein et al.*, 1957; *Chen et al.*, 2005; *Muschietti et al.*, 1999a, 1999b; *Ng and Bhattacharjee*, 2005]. They can be generated by the electron two-stream instability [*Morse and Nielson*, 1969] or the Buneman instability [*Drake et al.*, 2003]. Particle-in-cell (PIC) simulations have confirmed that electron holes can be formed in the two-stream instability, and these holes can persist for a sufficiently long time in one-dimensional (1D) PIC simulation (usually longer than several thousands of $\omega_{pe}^{-1}$, where $\omega_{pe}$ is electron plasma frequency) [*Omura et al.*, 1994; *Mottez et al.*, 1997; *Lu et al.*, 2005a, 2005b]. However, multidimensional PIC simulations have demonstrated that electron holes are unstable to the transverse instability [*Muschietti et al.*, 2000]. The transverse instability is due to the dynamics of the trapped electrons in electron holes and is a self-focusing type of instability. Perturbations in electron holes can produce transverse gradients of the electric potential. Such transverse gradients focus the trapped electrons into

[1]CAS Key Laboratory of Basic Plasma Physics, School of Earth and Space Sciences, University of Science and Technology of China, Hefei, China.
[2]State Key Laboratory of Space Weather, Chinese Academy of Sciences, Beijing, China.
[3]Institute of Geology and Geophysics, Chinese Academy of Sciences, Beijing, China.
[4]School of Physics, University of Science and Technology of China, Hefei, China.


0148-0227/11/2011JA016486

regions that already have a surplus of electrons, which leads to larger transverse gradients and more focusing. With the help of two-dimensional (2D) electrostatic PIC simulations, *Lu et al.* [2008] investigated the nonlinear evolution of electron holes in magnetized plasma, and found that such an evolution is governed by the combined actions between the transverse instability and the stabilization by the background magnetic field. In very weakly magnetized plasma ($\Omega_e \ll \omega_{pe}$, where $\Omega_e$ is the electron gyrofrequency), the parallel cut of the perpendicular electric field ($E_\perp$) has bipolar structures in electron holes, which have kinked structures. With the increase of the background magnetic field, the parallel cut of $E_\perp$ has unipolar structures in electron holes. In very strongly magnetized plasma ($\Omega_e \gg \omega_{pe}$), the unipolar structures of $E_\perp$ can last for thousands of electron plasma periods [*Wu et al.*, 2010]. The simulation results can explain the Polar and Fast observations in the auroral region, where the parallel cut of $E_\perp$ is measured to have unipolar structures in electron holes [*Ergun et al.*, 1998a, 1998b; *Franz et al.*, 1998, 2005; *Grabbe and Menietti*, 2006].

[4] Recently, *Andersson et al.* [2009] present the observations of magnetic field perturbations caused by electron holes in Earth's plasma sheet by the THEMIS satellites, and the fluctuating magnetic field is found to have regular structures. In this paper, we perform 2D electromagnetic PIC simulations to investigate the interactions between the transverse instability and the stabilization by the magnetic field in electron holes. The effects of the background magnetic field on the associated magnetic structures in electron holes are also studied. At last, we discuss the relevance between our simulation results and the observational characteristics of electron holes.

[5] The paper is organized as follows. In section 2, we describe the 2D electromagnetic PIC code. The simulation results are presented in section 3. The discussion and conclusions are given in section 4.

## 2. Simulation Model

[6] A 2D electromagnetic PIC code with periodic boundary conditions is employed in our simulations. The background magnetic field $\mathbf{B}_0$ is along the $x$ direction. In the simulations, ions are assumed infinitely massive and their dynamics are excluded. The electric and magnetic fields are obtained by integrating the time-dependent Maxwell equations, and a rigorous charge conservation scheme for the current deposition is employed in this model to ensure that $\nabla \cdot \mathbf{E} = \rho/\varepsilon_0$ (where $\rho$ is the charge density) is satisfied [*Villasenor and Buneman*, 1992]. Initially, a potential structure, which represents a one-dimensional electron hole, is located in the middle of the simulation domain. This potential is described as

$$\phi(x) = \psi \exp\left[-0.5(x-L)^2/\Delta_\parallel^2\right], \tag{1}$$

where $\Delta_\parallel$ and $L$ are the half width and center position of the electron hole, respectively, $\psi$ is the amplitude of the potential structure. The potential structure is homogeneous in the transverse direction, which is supported by a clump of trapped electrons in the electron hole. The trapped electrons gyrate in the background magnetic field, and simultaneously they bounce back and forth in the parallel direction. The motions of a trapped electron are determined by the ratio of the electron gyrofrequency $\Omega_e$ to the bounce frequency $\omega_b = \sqrt{\psi/\Delta_\parallel^2}$ [*Muschietti et al.*, 2000]. The initial electron distributions can be calculated by the BGK method self-consistently, which has already been given by *Muschietti et al.* [1999a, 1999b]. It is

$$F(x, v_x, v_y, v_z) = F_1(w) \exp\left[-0.5\left(v_y^2 + v_z^2\right)\Big/ v_{Te}^2\right], \tag{2}$$

where $v_{Te} = (T_e/m_e)^{1/2}$ is the electron thermal velocity, and $T_e$ is the electron temperature. $w \equiv v_x^2 - 2\phi(x)$ is twice the parallel energy and

$$F_1(w) = \frac{\sqrt{-w}}{\pi\Delta_\parallel^2}\left[1 + 2\ln\left(\frac{\psi}{-2w}\right)\right] + \frac{6 + \left(\sqrt{2} + \sqrt{-w}\right)(1-w)\sqrt{-w}}{\pi\left(\sqrt{2} + \sqrt{-w}\right)\left(4 - 2w + w^2\right)},$$

$$\text{For } -2\psi \le w < 0 \tag{3a}$$

$$F_1(w) = \frac{6\sqrt{2}}{\pi(8 + w^3)}. \text{ For } w > 0 \tag{3b}$$

Equations (3a) and (3b) describe the distributions of the trapped and passing electrons, respectively. The trapped electron distribution has a hollowed out shape, while the passing electron distribution has a flattop shape.

[7] In the simulations, the density is normalized to the unperturbed density $n_0$. The velocities are expressed in units of the electron thermal velocity $v_{Te}$. The dimensionless units used here have space in Debye length $\lambda_D = (\varepsilon_0 T_e/n_0 e^2)^{1/2}$, time in the inverse of the plasma frequency $\omega_{pe} = (n_0 e^2/m_e\varepsilon_0)^{1/2}$, and potential in $m_e v_{Te}^2/e$. The electric field is expressed in unit of $m_e\omega_{pe}v_{Te}/e$, and the magnetic field in unit of $m_e\omega_{pe}/e$. Grid size units $\lambda_D \times \lambda_D$ are used in the simulations, and the time step is $0.02\ \omega_{pe}^{-1}$. There are average 625 particles in each cell, and the number of cells is $128 \times 128$. In our simulations, the speed of light is chosen as $c/v_{Te} = 20.0$.

## 3. Simulation Results

[8] The evolution and associated electrostatic structures of electron holes have been extensively studied with 2D electrostatic simulations in previous work [*Oppenheim et al.*, 1999; *Lu et al.*, 2008; *Wu et al.*, 2010]. The evolution of electron holes is determined by the combined actions between the transverse instability and the stabilization by the background magnetic field. The background magnetic field guides the trapped electrons bounce back and forth in electron holes. It can prevent the trapped electrons from being focused by the transverse instability, and makes the electron hole stable [*Muschietti et al.*, 2000; *Lu et al.*, 2008; *Wu et al.*, 2010]. In this paper, we perform 2D self-consistent electromagnetic PIC simulations to investigate the evolution of electron holes. Our main interests are the effects of the background magnetic field and initial potential amplitude $\psi$ on the structures of the fluctuating magnetic field in the electron holes. A total of 5 runs are performed, and the parameters are listed in Table 1. In Run 1, $\Omega_e$ is set as 0.7,

**Table 1.** Summary of Simulations (Runs 1–5)

| Run | $\psi$ | $\Delta_\parallel$ | $\omega_b$ | $\Omega_e$ | $\Omega_e/\omega_b$ |
|---|---|---|---|---|---|
| 1 | 2.0 | 3.0 | 0.47 | 0.7 | 1.49 |
| 2 | 2.0 | 3.0 | 0.47 | 0.1 | 0.21 |
| 3 | 2.0 | 3.0 | 0.47 | 2.0 | 4.26 |
| 4 | 1.0 | 2.0 | 0.50 | 0.7 | 1.40 |
| 5 | 1.0 | 2.0 | 0.50 | 2.0 | 4.00 |

and the initial potential is characterized by $\psi = 2.0$ and $\Delta_\parallel = 3.0$. Compared with Run 1, $\Omega_e$ is changed to 0.1 and 2.0 in Run 2 and 3 to investigate the influence of the background magnetic field. Run 4–5, with $\psi = 1.0$ and $\Delta_\parallel = 2.0$, are performed to study the effects of the initial potential amplitude. The chosen parameters are consistent with both the observations [*Ergun et al.*, 1998a] and the theoretical prediction [*Muschietti et al.*, 1999a, 1999b].

[9] Run 1 corresponds to weakly magnetized plasma, and the electron gyrofrequency $\Omega_e$ is larger than the bounce frequency $\omega_b$. Figure 1 shows the overall evolution of the electric field energies $E_x^2$, $E_y^2$ and the fluctuating magnetic field energy $\delta B^2 = \delta B_x^2 + \delta B_y^2 + \delta B_z^2$ for Run 1. At about $\omega_{pe}t = 300$, with the excitation of the transverse instability, the electric field energy $E_x^2$ begins to decrease, while the fluctuating magnetic field energy $\delta B^2$ and electric field energy $E_y^2$ increase. The electric field energy $E_y^2$ attains its maximum value at about $\omega_{pe}t = 900$. We also find that in our simulations (Run 1–4) the total energy is almost conserved, and it changes less than 0.1%. Most of the initial electric field energy is transferred into the electron kinetic energy.

[10] The evolution of the electromagnetic field associated with the electron hole for Run 1 is shown in Figure 2, which plots $E_x$ (Figure 2a), $E_y$ (Figure 2b), $\delta B_x$ (Figure 2c), $\delta B_y$ (Figure 2d) and $\delta B_z$ (Figure 2e) at $\omega_{pe}t = 0$, 800, and 1340, respectively. With the excitation of the transverse instability, we can observed a quasi-1D electron hole with kinked structures, which is described at the time $\omega_{pe}t = 800$. Along the direction perpendicular to background magnetic field, a series of islands with alternate positive and negative values are formed for $E_y$, $\delta B_x$ and $\delta B_z$ in the electron hole, and their parallel cut along the magnetic field has unipolar structures. At the same time, we can also found regular structures for $\delta B_y$ in the electron hole, and their parallel cut along the magnetic field has bipolar structures. At last, The electron hole decays into several 2D electron holes as shown at the time $\omega_{pe}t = 1340$. The 2D electron holes are isolated in both the $x$ and $y$ directions. The parallel cut of $E_y$, $\delta B_x$ and $\delta B_z$ can be found to have unipolar structures in these electron holes, and $\delta B_x$ always has positive values. $\delta B_y$ can be observed to have quadrupole structures in the electron holes, whose parallel cut has bipolar structures.

[11] The electric structures associated with electron holes have already been explained previously [*Oppenheim et al.*, 1999; *Lu et al.*, 2008; *Wu et al.*, 2010], and the formation of such magnetic structures associated with the electron holes can be described as follows: due to the existence of the perpendicular electric fields $E_y$ in the electron holes, the trapped electrons in the electron holes will suffer the electric field drift along the $z$ direction, which can be expressed as $v_{Ez} \approx -E_y/B_0$. Therefore, the current along the $z$ direction is formed in the electron holes, which then generates the fluctuating magnetic field $\delta B_x$ and $\delta B_y$ associated with the electron holes [*Lu et al.*, 2008; *Wu et al.*, 2010]. The magnetic consequence of the current carried by the trapped electrons undergoing the electric field drift has previously been analyzed by *Umeda et al.* [2004].

[12] The structures of the drift velocity $v_{Ez}$ and the current along the $z$ direction $j_z$ at $\omega_{pe}t = 800$ and 1340 for Run 1 are depicted in Figure 3. We now model the patterns of current $j_z$ observed in the PIC simulations at $\omega_{pe}t = 800$ and 1340 with the following expression:

$$j_z = j_{z0}\exp\left[-0.5\left(\frac{(x-L_x)^2}{\Delta_x^2}+\frac{(y-36.0)^2}{\Delta_y^2}\right)\right] - j_{z0}\exp\left[-0.5\left(\frac{(x-L_x)^2}{\Delta_x^2}+\frac{(y-28.0)^2}{\Delta_y^2}\right)\right], \quad (4)$$

$$j_z = \sum_{i=0}^{7}(-1)^i j_{z0}\exp\left[-0.5\left(\frac{(x-L_x)^2}{\Delta_x^2}+\frac{(y-L_i)^2}{\Delta_y^2}\right)\right], \quad (5)$$

where $j_{z0} = 0.1$, $\Delta_x = \Delta_y = 3.0$, $L_x = 32.0$ and $L_i = 4 + 8i$ ($i = 0, 1 \cdots, 7$). The currents in equation (5) are also periodic

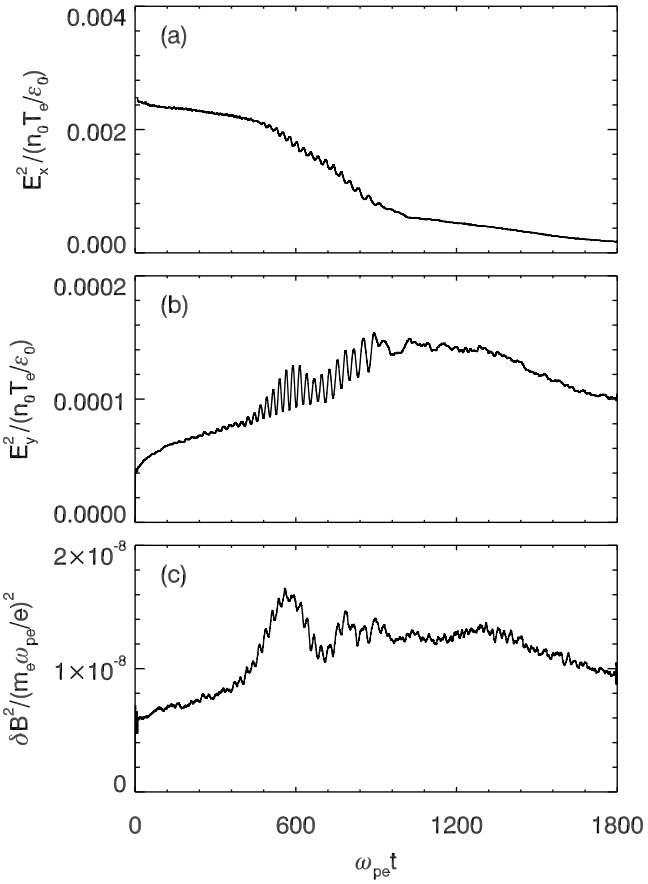


**Figure 1.** The time evolution of the electric field energies (a) $E_x^2$ and (b) $E_y^2$ and (c) the fluctuating magnetic field energy $\delta B^2 = \delta B_x^2 + \delta B_y^2 + \delta B_z^2$ for Run 1. The electric field energies are normalized by $n_0T_e/\varepsilon_0$, and the magnetic field energy is normalized by $\frac{m_e^2\omega_{pe}^2}{e^2}$.

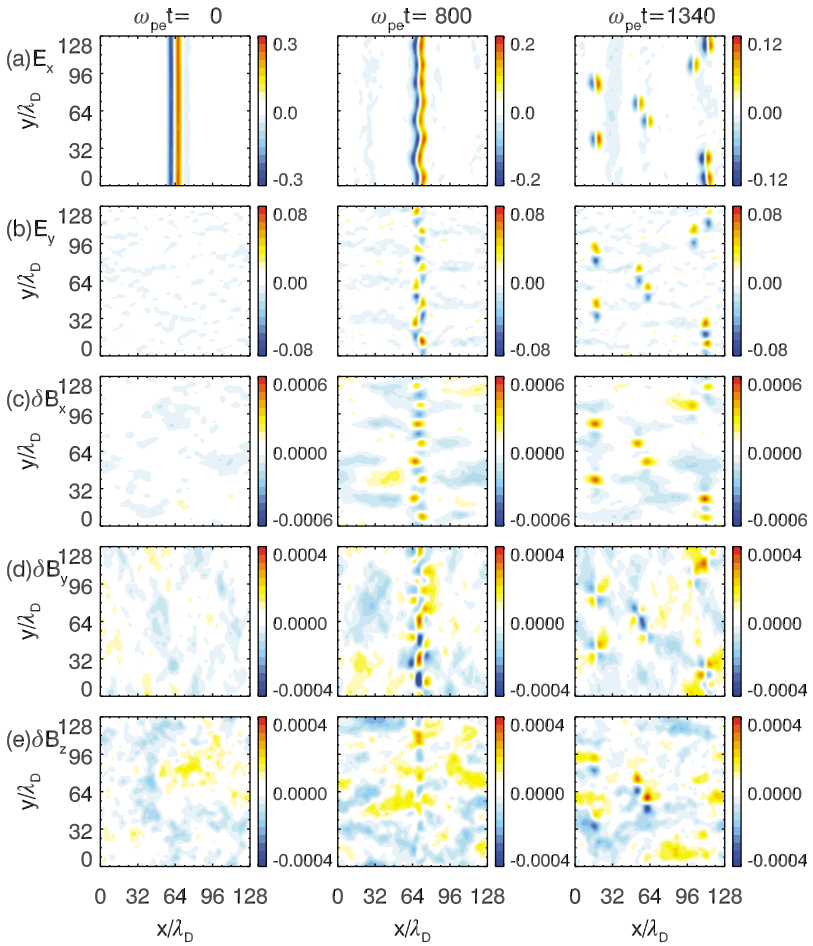


**Figure 2.** The electric field components (a) $E_x$ and (b) $E_y$ and the fluctuating magnetic field components (c) $\delta B_x$, (d) $\delta B_y$, and (e) $\delta B_z$ at $\omega_{pe}t$ = 0, 800 and 1340 for Run 1.

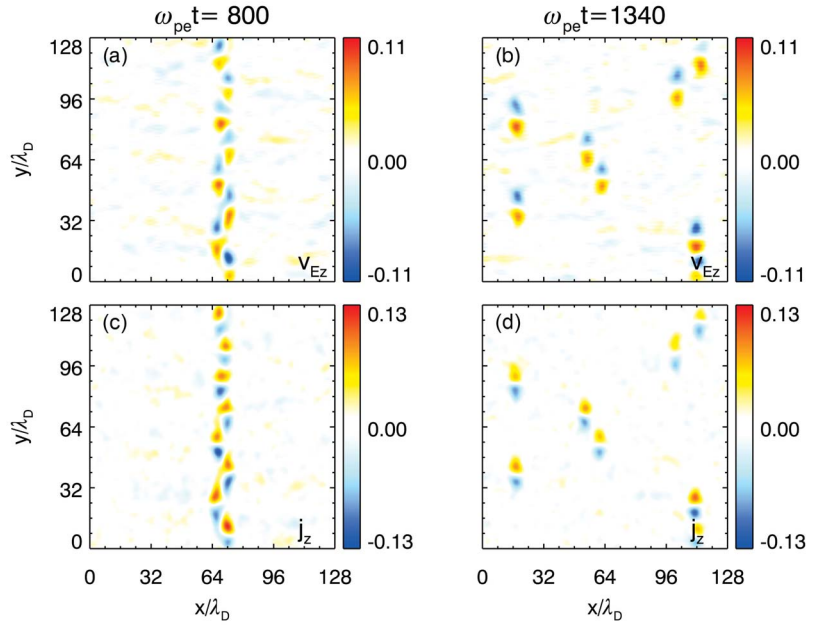


**Figure 3.** (a and b) The $z$ component of the $\vec{E} \times \vec{B}$ drift velocity at the time $\omega_{pe}t$ = 800 and 1340, and (c and d) the $z$ component of currents at the time $\omega_{pe}t$ = 800 and 1340.

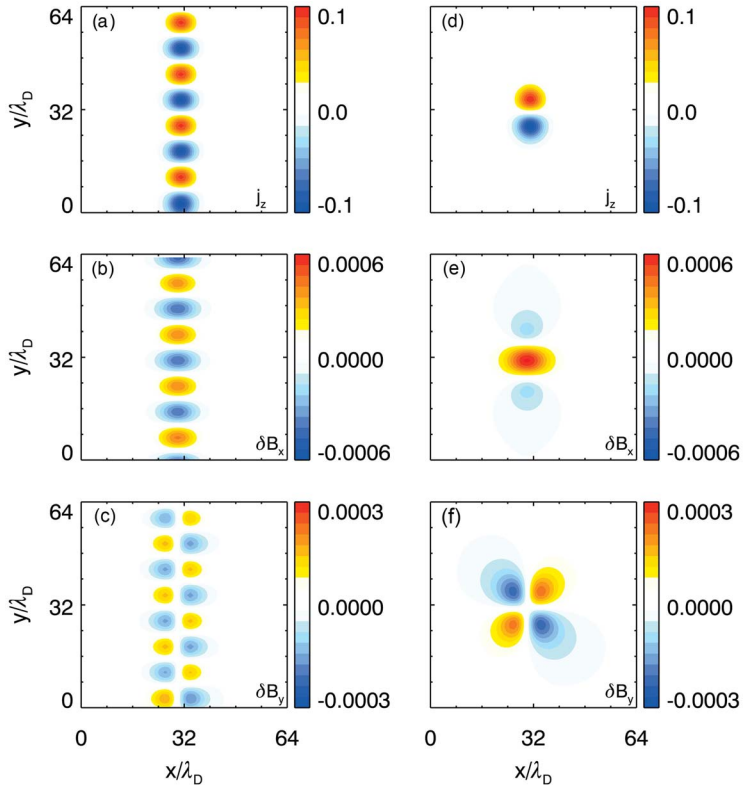


**Figure 4.** (a) Currents calculated by equation (4), and the fluctuating magnetic field (b) $\delta B_x$ and (c) $\delta B_y$ generated by the currents described in Figure 4a. (d) Currents calculated by equation (5), and the fluctuating magnetic field (e) $\delta B_x$ and (f) $\delta B_y$ generated by the currents described in Figure 4d.

along the $y$ direction as in the simulations. Figure 4 shows the structures of $\delta B_x$ and $\delta B_y$ generated by the currents described by equations (4) and (5). Their structures are similar to the currents in the simulations at $\omega_{pe}t$ = 800 and 1340 for Run 1. The fluctuating magnetic field $\delta B_x$ generated by such currents are depicted in Figures 4b and 4e, while $\delta B_y$ are depicted in Figures 4c and 4f. Obviously, the structures of the fluctuating magnetic field $\delta B_x$ and $\delta B_y$ in Figure 4 are similar to that in the simulation results in Run 1, which demonstrate the fluctuating magnetic field $\delta B_x$ and $\delta B_y$ are produced by the currents in the $z$ direction due to the electric field drift.

[13] The structures of the fluctuating magnetic field along the $z$ direction, whose parallel cut has unipolar structures, can be explained by a Lorentz transformation of a moving quasi-electrostatic structure [*Andersson et al.*, 2009]. The fluctuating magnetic field $\delta B_z$ can be described as

$$\delta B_z = \frac{v_{EH}}{c^2} E_y. \tag{6}$$

where $v_{EH}$ is the propagation velocity of the electron hole, which is parallel to the background magnetic field $\mathbf{B}_0$. With the excitation of the transverse instability, a quasi-1D kinked electron hole is formed. The oscillation and the

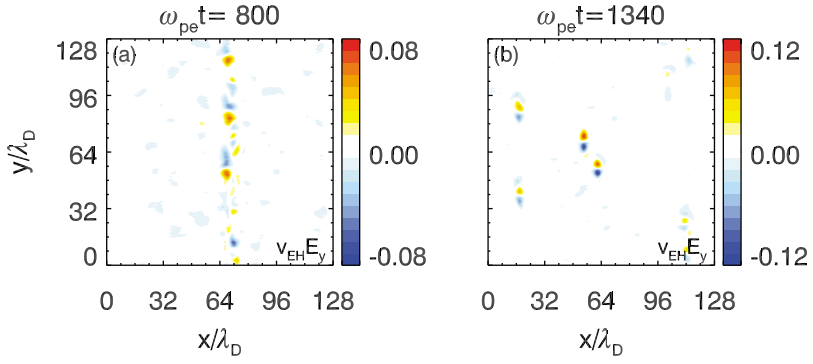


**Figure 5.** $v_{EH}E_y$ at the time $\omega_{pe}t$ = 800 and 1340 for Run 1.

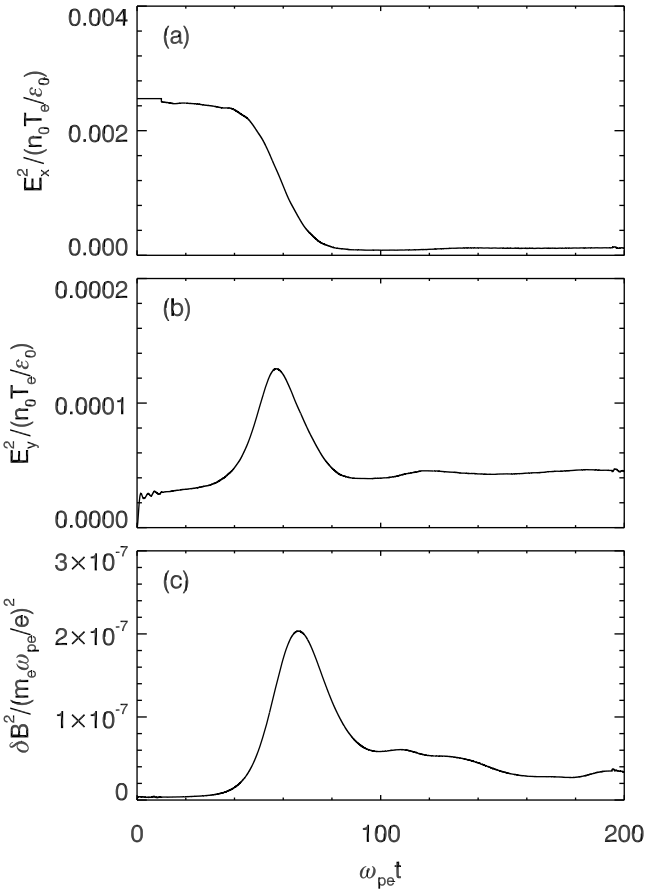


**Figure 6.** The time evolution of the electric field energies (a) $E_x^2$ and (b) $E_y^2$ and (c) the fluctuating magnetic field energy $\delta B^2 = \delta B_x^2 + \delta B_y^2 + \delta B_z^2$ for Run 2. The electric field energies are normalized by $n_0 T_e/\varepsilon_0$, and the magnetic field energy is normalized by $\frac{m_e^2 \omega_{pe}^2}{e^2}$.

existence of the perpendicular electric field $E_y$ produce the fluctuating magnetic field $\delta B_z$. At last, the quasi-1D electron hole is broken into several 2D electron holes, and these 2D holes propagate along the background magnetic field, which generates the fluctuating magnetic field $\delta B_z$. The generation mechanisms of the fluctuating magnetic field $\delta B_z$ can be demonstrated by Figure 5, which shows $v_{EH} E_y$ at the time $\omega_{pe} t$ = 800 and 1340 for Run 1, respectively. Please note, although in this run the propagation velocity of all the 2D electron holes is positive, it may also be negative.

[14] In Run 2 and Run 3, we investigate the effects of the background magnetic field on the magnetic structures associated with the electron holes. Run 2 corresponds to a weakly magnetized plasma where the electron gyrofrequency $\Omega_e$ is now smaller than the bounce frequency $\omega_b$. Run 3 corresponds to strongly magnetized plasma, where the electron gyrofrequency $\Omega_e$ is larger than both the bounce frequency $\omega_b$ and electron plasma frequency $\omega_{pe}$. Figure 6 shows the overall evolution of the electric field energies $E_x^2$, $E_y^2$ and the fluctuating magnetic field energy $\delta B^2 = \delta B_x^2 + \delta B_y^2 + \delta B_z^2$ for Run 2. Here, compared with Run 1, the transverse instability, which is excited at about $\omega_{pe} t = 40$, is easier to be excited due to the weaker background magnetic field. With the excitation of the transverse instability, $E_x^2$ begins to decrease while $E_y^2$ begins to increase. Meanwhile, the magnetic field energy $\delta B^2$ begins to increase, which reaches its maximum a little later than $E_y^2$. In very weakly magnetized plasma, the transverse instability dominates the evolution of electron holes. After the transverse instability is sufficiently strong, the electron holes begin to be destroyed. Figure 7 shows the evolution of the electromagnetic field associated with the electron hole for Run 2. Shown are $E_x$ (Figure 7a), $E_y$ (Figure 7b), $\delta B_x$ (Figure 7c), $\delta B_y$ (Figure 7d) and $\delta B_z$ (Figure 7e) at $\omega_{pe} t$ = 0, 52, and 58, respectively. With the excitation of the transverse instability, we can observed a quasi-1D kinked electron hole, and the parallel cut of the perpendicular electric field $E_y$ has bipolar structures. However, in this run, because the electron gyrofrequency is smaller than bounce frequency of the trapped electrons in the electron hole, the motions of the trapped electrons are nonadiabatic, and there is no obvious electric field drift along the $z$ direction. The structures of the fluctuating magnetic field $\delta B_x$ and $\delta B_y$ change quickly. At the same time, the oscillation and the existence of the perpendicular electric field $E_y$ produce the fluctuating magnetic field $\delta B_z$, as demonstrated in equation (6). After the electron hole is destroyed by the transverse instability, the electromagnetic structures of electron holes disappear.

[15] Figures 8 and 9 show the simulation results for Run 3. Figure 8 shows the overall evolution of the electric field energies $E_x^2$, $E_y^2$ and the fluctuating magnetic field energy $\delta B^2 = \delta B_x^2 + \delta B_y^2 + \delta B_z^2$ for Run 3. Figure 9 depicts the evolution of the electromagnetic field associated with the electron hole for Run 3. Shown are $E_x$ (Figure 9a), $E_y$ (Figure 9b), $\delta B_x$ (Figure 9c), $\delta B_y$ (Figure 9d) and $\delta B_z$ (Figure 9e) at $\omega_{pe} t$ = 0, 1430, and 2600, respectively. The evolutions of electric field energies and magnetic field energy are similar to Run 1. The difference is that with the excitation of the transverse instability electrostatic whistler waves with streaked structures of the perpendicular electric field $E_y$ are excited outside the electron hole. The electrostatic whistler waves are a generalization of Langmuir waves and often observed in the multidimensional PIC simulations of electron two-stream instabilities [*Oppenheim et al.*, 1999; *Goldman et al.*, 1999; *Lu et al.*, 2008]. As proposed by *Wu et al.* [2010] the generation mechanism of the electrostatic whistler waves can be described as follows: at first, the perpendicular electric field $E_y$ in the electron hole can influence the electron trajectories which pass through the electron hole, which leads to the variation of the charge density along the $y$ direction outside of the electron hole, and the streaked structures of $E_y$ are formed. Then, the interaction between the streaked structures of $E_y$ outside electron holes and the vibration of the kinked electron hole emit the electrostatic whistler waves. With the drift motion of electrons inside and outside electron holes, the currents along the $z$ direction $j_z$ are formed. The currents generates the fluctuating magnetic field $\delta B_x$ and $\delta B_y$. The structures of the drift velocity $v_{Ez}$ and the current $j_z$ at $\omega_{pe} t$ = 1430 and 2600 for Run 3 are depicted in Figure 10. Because of the streaked structures of the current $j_z$, the amplitude of $\delta B_y$ is much smaller than that of $\delta B_x$. The generation mechanism of the fluctuating magnetic field $\delta B_z$ is due to the propagation of the electrostatic whistler waves along the $x$ direction. According to equation (6), we can know that the propagating whistler

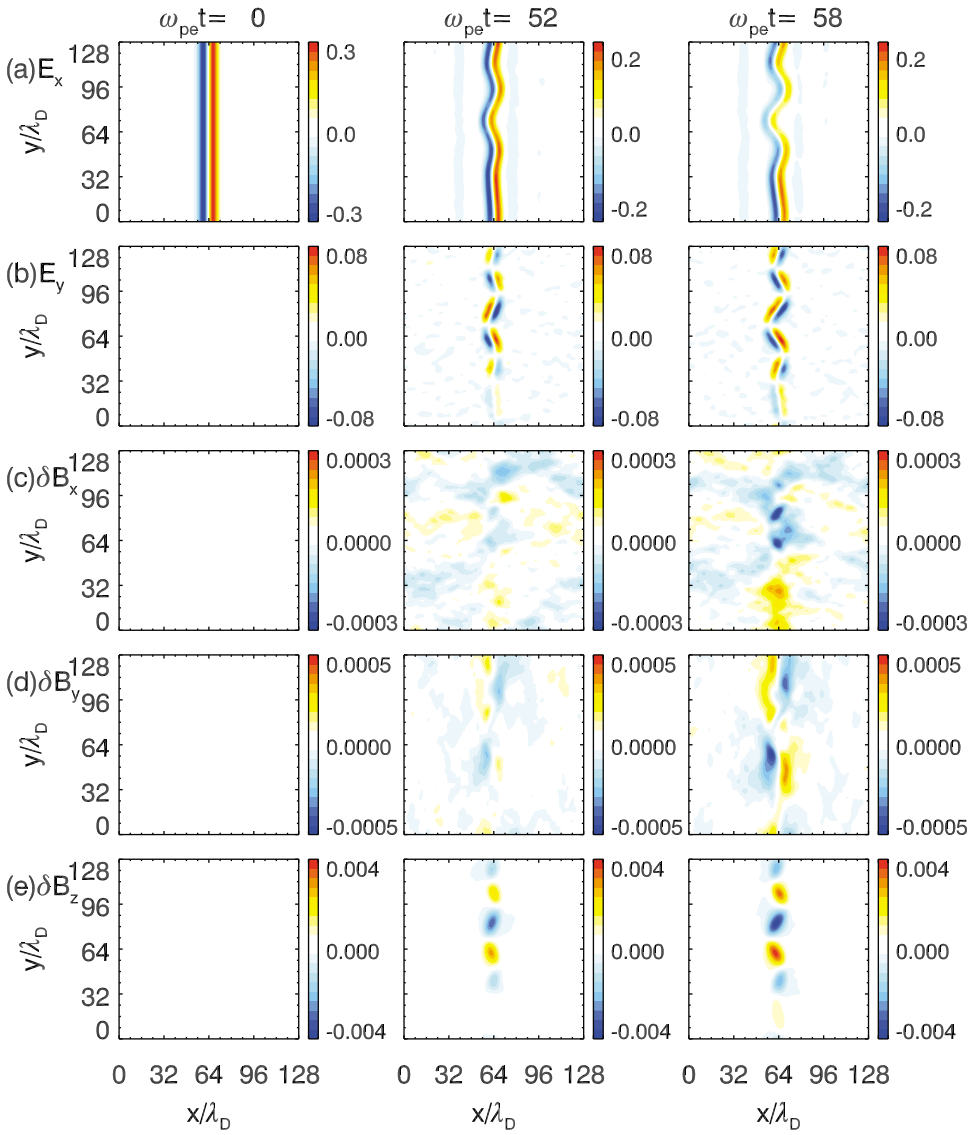


**Figure 7.** The electric field components (a) $E_x$ and (b) $E_y$ and the fluctuating magnetic field components (c) $\delta B_x$, (d) $\delta B_y$, and (e) $\delta B_z$ at $\omega_{pe}t$ = 0, 52 and 58 for Run 2.

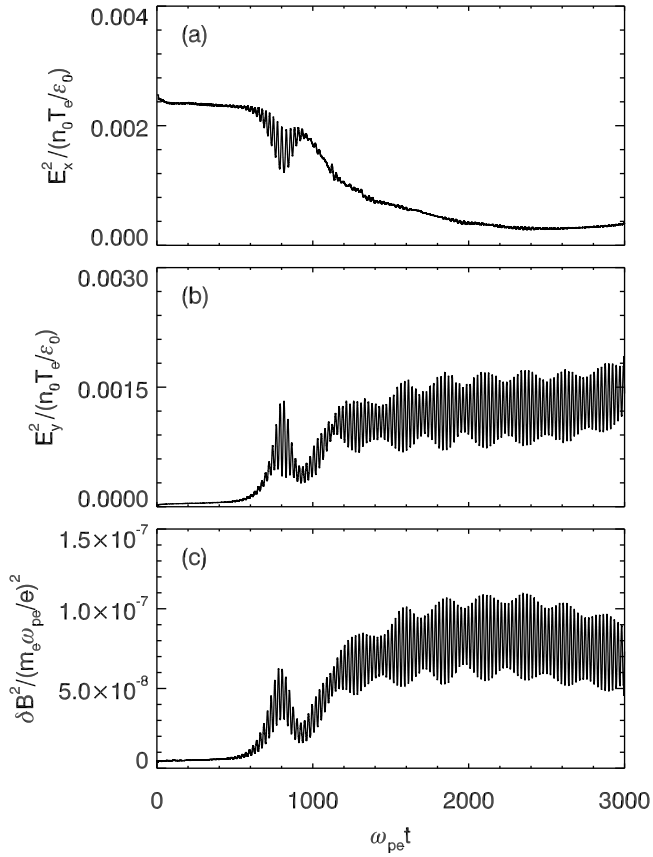


**Figure 8.** The time evolution of the electric field energies (a) $E_x^2$ and (b) $E_y^2$ and (c) the fluctuating magnetic field energy $\delta B^2 = \delta B_x^2 + \delta B_y^2 + \delta B_z^2$ for Run 3. The electric field energies are normalized by $n_0T_e/\varepsilon_0$, and the magnetic field energy is normalized by $\frac{m_e^2\omega_{pe}^2}{e^2}$.

waves can produce the streaked structures of the fluctuating magnetic field $\delta B_z$, as shown in Figure 10.

[16] We also change the initial potential amplitude $\psi$ to investigate the effects on the structures of the fluctuating magnetic field, which is demonstrated with Run 4 and 5. Figures 11 and 12 show $E_x$ (Figures 11a and 12a), $E_y$ (Figures 11b and 12b), $\delta B_x$ (Figures 11c and 12c), $\delta B_y$ (Figures 11d and 12d) and $\delta B_z$ (Figures 11e and 12e) at different times for Run 4 and 5, respectively. Compared with Run 1 and 3, the evolutions are similar. However, the amplitude of the fluctuating magnetic field is much weaker. If we decrease the initial potential amplitude $\psi$ further, the fluctuating magnetic field will be too weak to be observed.

## 4. Discussion and Conclusions

[17] In summary, we perform 2D electromagnetic PIC simulations to study the structures of the fluctuating magnetic field in electron holes. In very weakly magnetized plasma, the fluctuating magnetic field associated with the electron hole disappears quickly. When $\Omega_e$ is comparable to $\omega_{pe}$, at first a kinked electron hole is formed. In the electron hole, the parallel cut of the fluctuating magnetic field $\delta B_x$ and $\delta B_z$ has unipolar structures, while the parallel cut of the fluctuating magnetic field $\delta B_y$ has bipolar structures. At last, the electron hole is broken into several 2D electron holes. In these electron holes, the parallel cut of the fluctuating magnetic field $\delta B_x$ and $\delta B_z$ has unipolar structures and $\delta B_x$ always has positive value, while $\delta B_y$ has quadrupole structures and its parallel cut has bipolar structures. In strongly magnetized plasma, the electrostatic whistler waves with streaked structures of $E_y$ are excited, and the fluctuating magnetic field $\delta B_x$ and $\delta B_z$ generated by $E_y$ also has streaked structures, although the amplitude of $\delta B_y$ is very small. The structures of the fluctuating magnetic field $\delta B_x$ and $\delta B_y$ are generated by the current in the $z$ direction produced by the electric field drift due to the existence of $E_y$. The fluctuating magnetic field $\delta B_z$ is due to the Lorentz-transformed $E_y$ of a 2D electron hole moving along the direction of the background magnetic field. The magnetic structures associated with the electron holes disappear when the initial potential is sufficiently smaller. We should note that the effects of ion dynamics on the evolution of an electron hole are neglected in the present study. However, how it will influence the magnetic structures associated with the electron hole is beyond the scope of this paper, and needs further investigations.

[18] From the experiment viewpoint, features of the magnetic structures associated with electron holes have been observed by the THEMIS mission in Earth's plasma sheet [*Andersson et al.*, 2009]. In the observation results, both the parallel fluctuating magnetic field $\delta B_x$ and the perpendicular fluctuating magnetic field $\delta B_z$ associated electron holes have unipolar structures. In addition, the observations also show that such magnetic structures can only been found when the potential of the electron holes is sufficiently strong ($\psi \sim T_e/e$), and $\Omega_e/\omega_{pe}$ is about 0.8. All these observations are consistent with our simulation results.

[19] Inconsistent with the observations, our simulations demonstrate that $\delta B_y$ has bipolar structures while in the observations the parallel cut of $\delta B_y$ shows unipolar structures similarly to $\delta B_z$. The difference can be explained by the three-dimensional (3D) effects. If we assume that a 3D electron hole is cylindrically symmetric around the background magnetic field as in the model of *Muschietti et al.* [2002], then a parallel cut of $E_z$ will also show unipolar structures similarly to $E_y$ in the 2D simulations. At the same time, the current in the $z$ direction produced by the electric field drift due to the existence of $E_y$ in a 2D electron hole, is equivalent to an azimuthal current in the 3D geometry. Such a current will generate quadrupolar structures of $\delta B_y$ in the ($x$, $y$) plane, and the parallel cut of $\delta B_y$ will show bipolar structures in the hole, as in our 2D PIC simulations. At the same time, if the 3D electron hole moves along the background magnetic field, the components $E_y$ and $E_z$ which have unipolar structures in the 3D geometry will generate unipolar structures of $\delta B_y$ and $\delta B_z$ through the Lorentz transformation. Which contribution dominates and what structures of $\delta B_y$ are going to be observed depends critically upon the propagation speed of the hole. If the propagating speed is sufficiently large, we should observe the unipolar structures of $\delta B_y$, as shown in the observations. Otherwise, the bipolar structures of $\delta B_y$ should dominate, as described in our simulations.

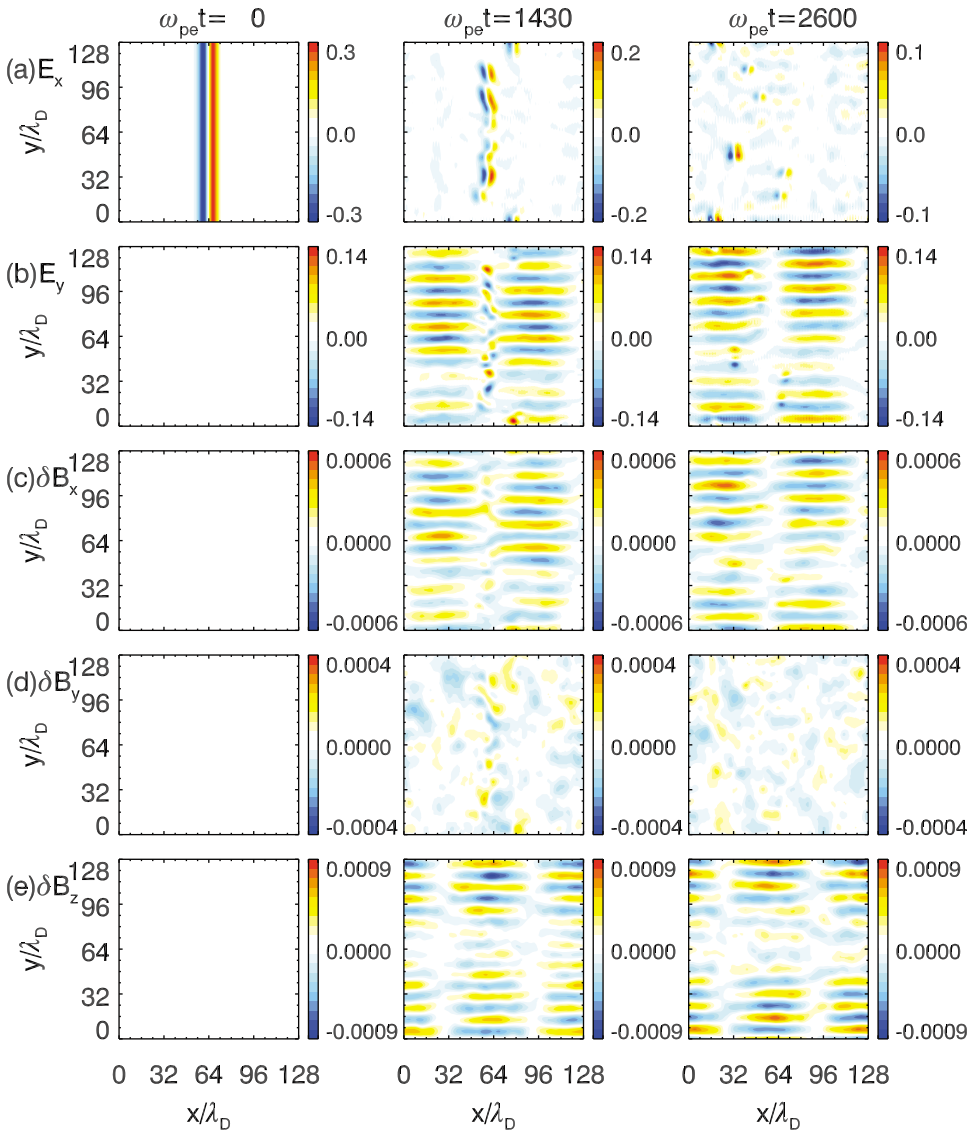


**Figure 9.** The electric field components (a) $E_x$ and (b) $E_y$ and the fluctuating magnetic field components (c) $\delta B_x$, (d) $\delta B_y$, and (e) $\delta B_z$ at $\omega_{pe}t$ = 0, 1430 and 2600 for Run 3.

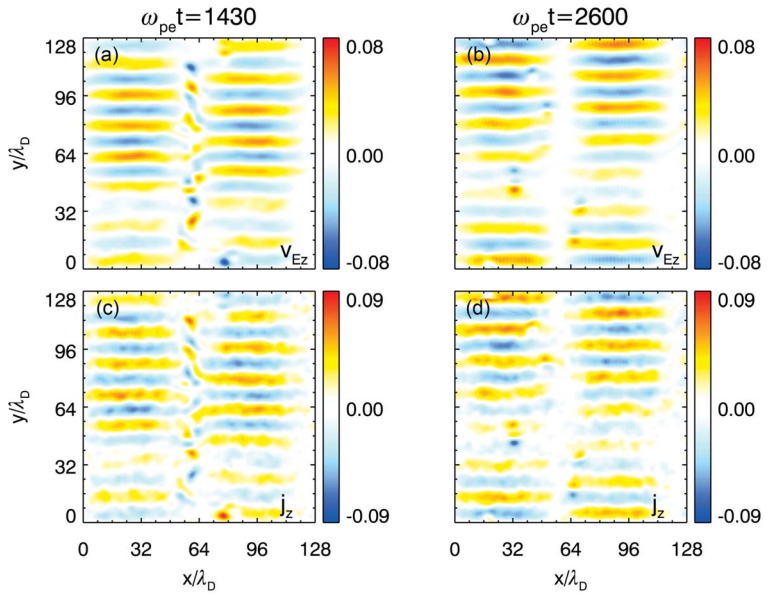


**Figure 10.** (a and b) The $z$ component of the $\vec{E} \times \vec{B}$ drift velocity at the time $\omega_{pe}t$ = 1430 and 2600 for Run 3, and (c and d) the $z$ component of currents at the time $\omega_{pe}t$ = 1430 and 2600 for Run 3.

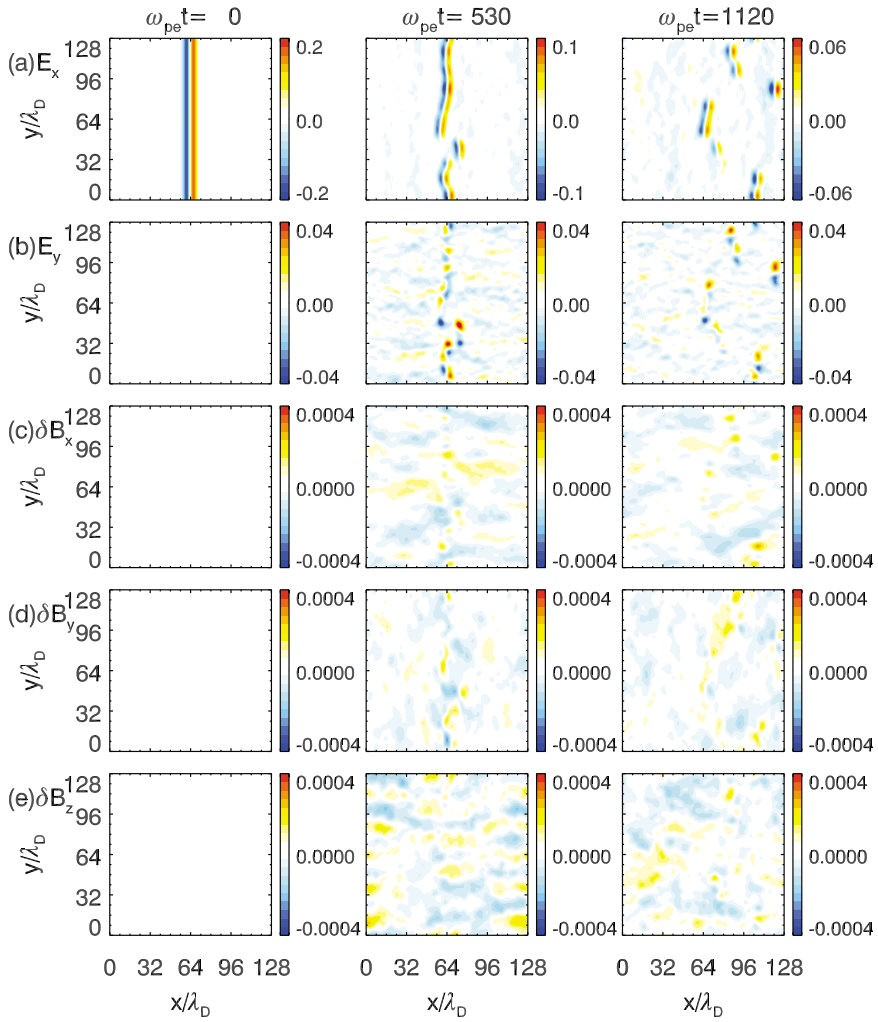


**Figure 11.** The electric field components (a) $E_x$ and (b) $E_y$ and the fluctuating magnetic field components (c) $\delta B_x$, (d) $\delta B_y$, and (e) $\delta B_z$ at $\omega_{pe}t$ = 0, 530 and 1120 for Run 4.

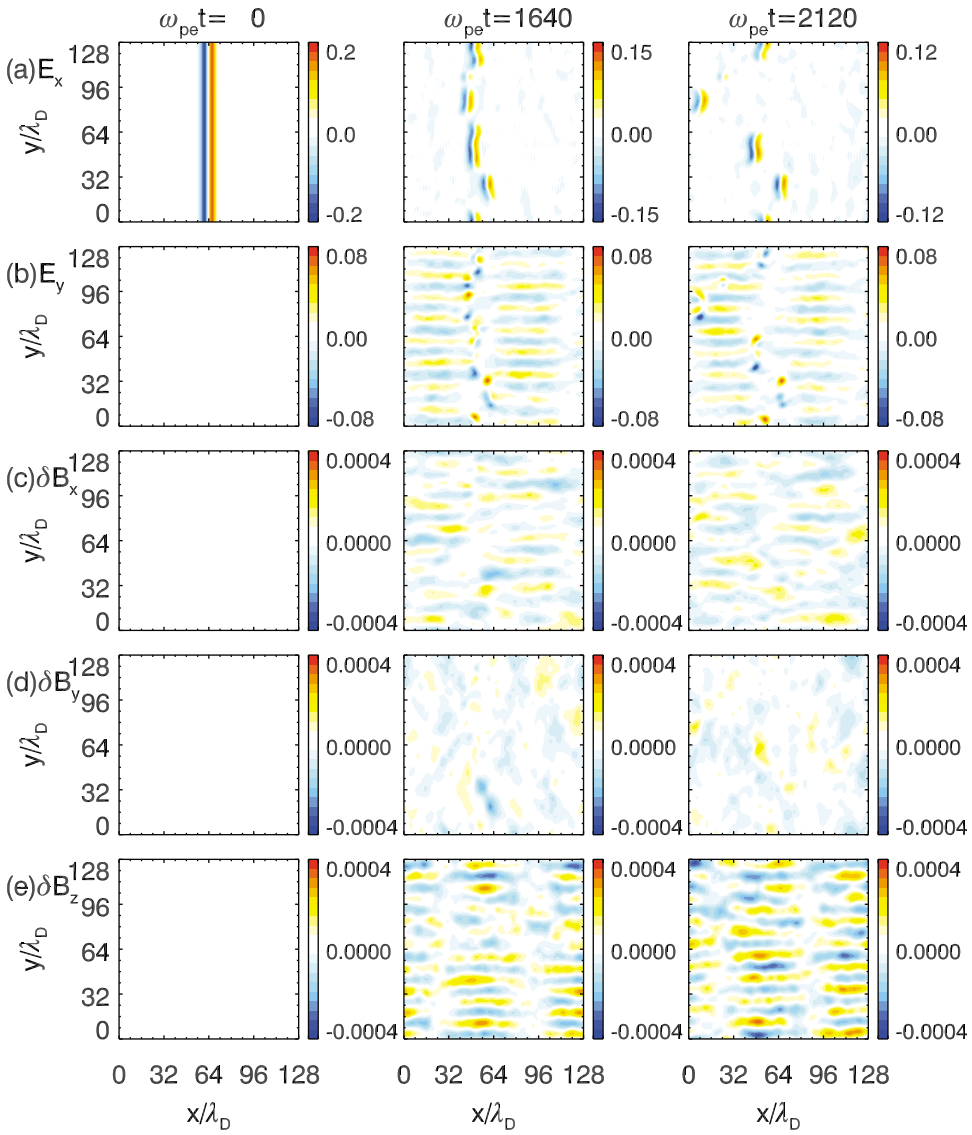


**Figure 12.** The electric field components (a) $E_x$ and (b) $E_y$ and the fluctuating magnetic field components (c) $\delta B_x$, (d) $\delta B_y$, and (e) $\delta B_z$ at $\omega_{pe}t$ = 0, 1640 and 2120 for Run 5.

[20] **Acknowledgments.** This research was supported by the National Science Foundation of China (NSFC) under grants 40974081, 40725013, 40931053, the Specialized Research Fund for State Key Laboratories, and the Fundamental Research Funds for the Central Universities (WK2080000010).

[21] Philippa Browning thanks the reviewers for their assistance in evaluating this paper.

## References

Andersson, L., et al. (2009), New features of electron phase space holes observed by the THEMIS mission, *Phys. Rev. Lett.*, *102*, 225004, doi:10.1103/PhysRevLett.102.225004.

Bale, S. D., P. J. Kellogg, D. E. Larson, R. P. Lin, K. Gpetz, and R. P. Lepping (1998), Bipolar electrostatic structures in the shock transition region: Evidence of electron phase holes, *Geophys. Res. Lett.*, *25*, 2929–2932, doi:10.1029/98GL02111.

Bernstein, I. B., J. M. Greene, and M. D. Kruskal (1957), Exact nonlinear plasma oscillations, *Phys. Rev.*, *108*, 546–550, doi:10.1103/PhysRev.108.546.

Cattell, C., J. Crumley, J. Dombeck, J. Wygant, and F. S. Mozer (2002), Polar observations of solitary waves at Earth's magnetopause, *Geophys. Res. Lett.*, *29*(5), 1065, doi:10.1029/2001GL014046.

Chen, L. J., J. Pickett, P. Kintner, J. Franz, and D. Gurnett (2005), On the width-amplitude inequality of electron phase space holes, *J. Geophys. Res.*, *110*, A09211, doi:10.1029/2005JA011087.

Drake, J. F., M. Swisdak, C. Cattell, M. A. Shay, B. N. Rogers, and A. Zeiler (2003), Formation of electron holes and particle energization during magnetic reconnection, *Science*, *299*, 873–877, doi:10.1126/science.1080333.

Ergun, R. E., et al. (1998a), Debye-scale plasma structures associated with magnetic-field-aligned electric fields, *Phys. Rev. Lett.*, *81*, 826–829, doi:10.1103/PhysRevLett.81.826.

Ergun, R. E., et al. (1998b), Fast satellite observations of large-amplitude solitary structures, *Geophys. Res. Lett.*, *25*, 2041–2044, doi:10.1029/98GL00636.

Fox, W., M. Porkolab, J. Egedal, N. Katz, and A. Le (2008), Laboratory observation of electron phase-space holes during magnetic reconnection, *Phys. Rev. Lett.*, *101*, 255003, doi:10.1103/PhysRevLett.101.255003.

Franz, J. R., P. M. Kintner, and J. S. Pickett (1998), POLAR observations of coherent electric field structures, *Geophys. Res. Lett.*, *25*, 1277–1280, doi:10.1029/98GL50870.

Franz, J. R., P. M. Kintner, J. S. Pickett, and L. J. Chen (2005), Properties of small-amplitude electron phase-space holes observed by Polar, *J. Geophys. Res.*, *110*, A09212, doi:10.1029/2005JA011095.

Goldman, M. V., M. M. Oppenheim, and D. L. Newman (1999), Nonlinear two-stream instabilities as an explanation for auroral bipolar wave structures, *Geophys. Res. Lett.*, *26*, 1821–1824, doi:10.1029/1999GL900435.

Grabbe, C. L., and J. D. Menietti (2006), Broadband electrostatic wave observations in the auroral region on Polar and comparisons with theory, *J. Geophys. Res.*, *111*, A10226, doi:10.1029/2006JA011602.

Lu, Q. M., D. Y. Wang, and S. Wang (2005a), Generation mechanism of electrostatic solitary waves in the Earth's auroral region, *J. Geophys. Res.*, *110*, A03223, doi:10.1029/2004JA010739.

Lu, Q. M., S. Wang, and X. K. Dou (2005b), Electrostatic waves in an electron-beam plasma system, *Phys. Plasmas*, *12*, 072903, doi:10.1063/1.1951367.

Lu, Q. M., B. Lembege, J. B. Tao, and S. Wang (2008), Perpendicular electric field in two-dimensional electron phase-holes: A parameter study, *J. Geophys. Res.*, *113*, A11219, doi:10.1029/2008JA013693.

Mangeney, A., C. Salem, C. Lacombe, J. L. Bougeret, C. Perche, R. Manning, P. J. Kellogg, K. Goetz, S. J. Monson, and J. M. Bosqued (1999), WIND observations of coherent electrostatic waves in the solar wind, *Ann. Geophys.*, *17*, 307–320, doi:10.1007/s00585-999-0307-y.

Matsumoto, H., H. Kojima, T. Miyatake, Y. Omura, M. Okada, I. Nagano, and M. Tsutsui (1994), Electrostatic solitary waves (ESW) in the magnetotail: BEN wave forms observed by Geotail, *Geophys. Res. Lett.*, *21*, 2915–2918, doi:10.1029/94GL01284.

Morse, R. L., and C. W. Nielson (1969), One, two-, and three-dimensional numerical simulation of two-beam plasmas, *Phys. Rev. Lett.*, *23*, 1087–1090, doi:10.1103/PhysRevLett.23.1087.

Mottez, F., S. Perraut, A. Roux, and P. Louarn (1997), Coherent structures in the magnetotail triggered by counterstreaming electron beams, *J. Geophys. Res.*, *102*(A6), 11,399–11,408, doi:10.1029/97JA00385.

Muschietti, L., R. E. Ergun, I. Roth, and C. W. Carlson (1999a), Phase-space electron holes along magnetic field lines, *Geophys. Res. Lett.*, *26*, 1093–1096.

Muschietti, L., R. E. Ergun, I. Roth, and C. W. Carlson (1999b), Correction to "Phase-space electron holes along magnetic field lines," *Geophys. Res. Lett.*, *26*, 1689, doi:10.1029/1999GL900302.

Muschietti, L., I. Roth, C. W. Carlson, and R. E. Ergun (2000), Transverse instability of magnetized electron holes, *Phys. Rev. Lett.*, *85*, 94–97, doi:10.1103/PhysRevLett.85.94.

Muschietti, L., I. Roth, C. W. Carlson, and M. Berthomier (2002), Modeling stretched solitary waves along magnetic field lines, *Nonlinear Processes Geophys.*, *9*, 101–109, doi:10.5194/npg-9-101-2002.

Newman, D. L., M. V. Goldman, R. E. Ergun, and A. Mangeney (2001), Formation of double layers and electron holes in a current-driven space plasma, *Phys. Rev. Lett.*, *87*, 255001, doi:10.1103/PhysRevLett.87.255001.

Ng, C. S., and A. Bhattacharjee (2005), Bernstein-Greene-Kruskal modes in a three-dimensional plasma, *Phys. Rev. Lett.*, *95*, 245004, doi:10.1103/PhysRevLett.95.245004.

Omura, Y., H. Kojama, and H. Matsumoto (1994), Computer simulation of electrostatic solitary waves: A nonlinear model of broadband electrostatic noise, *Geophys. Res. Lett.*, *21*, 2923–2926, doi:10.1029/94GL01605.

Oppenheim, M., D. L. Newman, and M. V. Goldman (1999), Evolution of electron phase-space holes in a 2D magnetized plasma, *Phys. Rev. Lett.*, *83*, 2344–2347, doi:10.1103/PhysRevLett.83.2344.

Pickett, J. S., L. J. Chen, S. W. Kahler, O. Santolik, D. A. Gurnett, B. T. Tsurutani, and A. Balogh (2004), Isolated electrostatic structures observed throughout the cluster orbit: Relationship to magnetic field strength, *Ann. Geophys.*, *22*, 2515–2523, doi:10.5194/angeo-22-2515-2004.

Saeki, K., P. Michelsen, H. L. Pecseli, and J. J. Rasmussen (1979), Formation and coalescence of electron solitary holes, *Phys. Rev. Lett.*, *42*, 501–504, doi:10.1103/PhysRevLett.42.501.

Sarri, G., et al. (2010), Observation and characterization of laser-driven phase space electron holes, *Phys. Plasmas*, *17*, 010701, doi:10.1063/1.3286438.

Umeda, T., Y. Omura, and H. Matsumoto (2004), Two-dimensional particle simulation of electromagnetic field signature associated with electrostatic solitary waves, *J. Geophys. Res.*, *109*, A02207, doi:10.1029/2003JA010000.

Villasenor, J., and O. Buneman (1992), Rigorous charge conservation for local electromagnetic field solvers, *Comput. Phys. Commun.*, *69*, 306–316, doi:10.1016/0010-4655(92)90169-Y.

Wu, M. Y., Q. M. Lu, C. Huang, and S. Wang (2010), Transverse instability and perpendicular electric field in two-dimensional electron phase-space holes, *J. Geophys. Res.*, *115*, A10245, doi:10.1029/2009JA015235.

A. Du, Institute of Geology and Geophysics, Chinese Academy of Sciences, Beijing 100029, China.

Q. Lu, S. Wang, and M. Wu, CAS Key Laboratory of Basic Plasma Physics, School of Earth and Space Sciences, University of Science and Technology of China, Hefei 230026, China. (qmlu@ustc.edu.cn)

J. Xie, School of Physics, University of Science and Technology of China, Hefei 230026, China.